Cloud Properties Simulated by a Single-Column Model. Part II: Evaluation of Cumulus Detrainment and Ice-phase Microphysics Using a Cloud Resolving Model

Yali Luo

National Institute of Aerospace, Hampton, VA

Steven K. Krueger

Department of Meteorology, University of Utah, Salt Lake City, Utah

Kuan-Man Xu

NASA Langley Research Center, Hampton, VA

October 26, 2005

Corresponding author:

Dr. Yali Luo

National Institute of Aerospace

100 Exploration Way, Hampton, VA 23666-6147

Email: yali@nianet.org

Phone: 757-325-6906 Fax: 757-325-6979

Abstract

This paper is the second in a series in which kilometer-scale-resolving observations from the Atmospheric Radiation Measurement program and a cloud-resolving model (CRM) are used to evaluate the single-column model (SCM) version of the National Centers for Environmental Prediction Global Forecast System model. Part I demonstrated that kilometer-scale cirrus properties simulated by the SCM significantly differ from the cloud radar observations while the CRM simulation reproduced most of the cirrus properties as revealed by the observations. The present study describes an evaluation, through a comparison with the CRM, of the SCM's representation of detrainment from deep cumulus and ice-phase microphysics in an effort to better understand the findings of Part I.

It is found that detrainment occurs too infrequently at a single level at a time in the SCM, although the detrainment rate averaged over the entire simulation period is somewhat comparable to that of the CRM simulation. Relatively too much detrained ice is sublimated when first detrained. Snow falls over too deep of a layer due to the assumption that snow source and sink terms exactly balance within one time step in the SCM. These characteristics in the SCM parameterizations may explain many of the differences in the cirrus properties between the SCM and the observations (or between the SCM and the CRM). A possible improvement for the SCM consists of the inclusion of multiple cumulus cloud types as in the original Arakawa-Schubert scheme, prognostically determining the stratiform cloud fraction and snow mixing ratio. This would allow better representation of the detrainment from deep convection, better coupling of the volume of detrained air with cloud fraction, and better representation of snow field.

1. Introduction

Most of the global weather prediction and climate models (hereafter, large-scale models) implement predictive equations for stratiform cloud condensate to couple cloud microphysical with dynamical processes. Detrainment of cloud condensate from cumulus convection is added as a source term to the grid-mean stratiform cloud mass. Cloud microphysical schemes as complicated as those used in much higher-resolution models, such as cloud-resolving models (CRMs), are used to represent the phase change among various species of water. Despite the increasing complexity of parameterizations of cloud-related processes in large-scale models in the past decade, clouds remain one of the major sources of uncertainties for projections of future climate (e.g. IPCC 2001). Improving the accuracy of their treatment in large-scale models is therefore essential for a realistic projection of future climate and an improved prediction of weather. Model evaluation is the first logical step towards improvement.

Observations of cloud properties are of the utmost importance for evaluating a model's performance, especially those observations which can reveal cloud variabilities on their native scale that result from interactions among dynamics, radiation, and microphysics. For example, the Atmospheric Radiation Measurement (ARM) program has been collecting continuous measurements of clouds and radiation with very high temporal resolution (a few minutes or less) at three sites (Stokes and Schwartz 1994). Various algorithms have been developed and applied to retrieve cloud microphysical properties from measurements obtained by instruments (e.g. Mace et al. 2001; Dong and Mace 2003). Satellites provide global observations and retrievals of cloud macrophysical and radiative properties such as cloud-top temperature/height, outgoing longwave radiative flux, albedo, cloud optical depth, cloud ice/liquid water path (e.g. Rossow and Schiffer 1991; Rossow et al. 1996).

While extremely useful for model evaluation, observations alone can hardly provide detailed information on processes influencing cloud variabilities such as detrainment from cumulus. Models which explicitly simulate individual cloud elements such as large-eddy simulation (LES) models and CRMs are useful tools to advance our understanding of various cloud processes and to evaluate and possibly to improve parameterizations used in global models (e.g. Randall et al. 1996, 2003). A major limitation of the CRMs is that radiative, microphysical, and turbulent processes must be parameterized. However, a CRM explicitly represents mesoscale and cloud-scale dynamics and hydrometeor fields (mixing ratios of hydrometeors) are predicted at a resolution of ~1 km in the horizontal and ~100 m in the vertical. An explicit interaction among dynamics, microphysics, and radiation operates at a fine spatial and temporal scale. However, assumptions about overlap and horizontal homogeneity of hydrometeor fields are necessary to calculate the change of the prognostic variables caused by radiative and microphysical processes in a lower-resolution model. These assumptions result in more uncertainties. Therefore, one can carefully use CRMs to evaluate the assumptions and parameterizations used in lower-resolution models, subject to the limitations of CRMs.

In this series of studies, we used a time-varying large-scale forcing data generated by the ARM program using the variational analysis method of Zhang et al. (1997, 2001) to drive the UCLA/CSU CRM (Krueger 1988) and a single-column model (SCM) version of the National Centers for Environmental Prediction (NCEP) Global Forecast System (GFS) model. The forcing data cover the summer 1997 Intensive Operation Period (IOP) at the ARM Southern Great Plains (SGP) site. Results from the two models were previously used to evaluate the simulated cirrus properties and physical processes through a comparison with the kilometer-scale-resolving observations/retrievals obtained from the ARM cloud radar. The CRM was found to reproduce

most features as revealed by the observations (Luo et al. 2003). We then used both the kilometer-scale-resolving observations and the CRM results to evaluate the SCM in this series of studies in order to demonstrate our new evaluation method.

In Part I (Luo et al. 2005), synthetic subgrid-scale (SGS) cloud fields were generated by applying the SCM's assumptions of cloud overlap and cloud horizontal inhomogeneity to its profiles of cloud fraction and cloud water/ice mixing ratio. Three sets of SCM synthetic SGS cloud fields were analyzed. Precipitating ice was included as part of cirrus for a randomly overlapped cirrus cloud field but it was excluded for the other two cirrus cloud fields which were either randomly or maximally/randomly overlapped. The cirrus statistics from the SCM were compared to a millimeter-wave cloud radar (MMCR) observations and retrievals produced by Mace et al. (2001) as well as results from the CRM simulation. Most aspects of the SGS SCM cirrus properties differ significantly from those observed by the MMCR and simulated by the CRM. The frequency distributions of the SCM cirrus cloud-base height and physical thickness depend on the assumption about cloud overlap and more significantly on whether precipitating ice is considered as part of cirrus clouds. Compared to the MMCR observations, there are too many cirrus layers that are thinner than 2 km (i.e. occupy only a single model layer), and the SCM cirrus cloud base heights are about right if precipitating ice is excluded as a part of cirrus clouds, but the cirrus base heights are too low and cloud thicknesses too large *if precipitating ice is included as a part of cirrus clouds*. Regardless of the overlap assumption used and whether precipitating ice is included or not, the distributions of ice water path (IWP) and layer-mean ice water content (IWC) of the SCM cirrus clouds are more skewed to large values than observed, and the layer-mean IWCs decrease with increasing cloud physical depth rather than increase as is observed (Mace et al. 2001).

Cloud microphysical processes, cumulus detrainment, large-scale advection, and turbulence directly determine the evolution of cloud condensate in an SCM. In the SCM simulation, the large-scale horizontal advection of cloud condensate is not included, due to lack of observations. The large-scale vertical advection of cloud condensate is implicitly given by assuming a balance between the upward transport by large-scale motion and sedimentation. We therefore expect that the cirrus properties are closely related to cumulus detrainment and microphysical processes in the model. Since no observational data of detrainment and ice-phase microphysical conversion rates were available and the CRM cirrus statistics agreed well with the observations, we compared the SCM with the CRM with a focus on the representations of cumulus detrainment and ice-phase microphysical processes in the present study. Our evaluation method and results are described subsequently.

To evaluate the SCM's representation of cumulus detrainment and subsequent sublimation of cloud ice through microphysical parameterization, we analyzed and compared the results from 29-day simulations by the CRM and SCM. Detailed descriptions of the model and simulation were provided in Luo et al. (2003) for the CRM and in Luo et al. (2005) for the SCM, respectively. To evaluate the assumptions of precipitating ice and ice-phase microphysical parameterizations in the SCM, we developed a 1-D microphysics-only model implemented with either the SCM or the CRM ice-phase microphysical scheme. The temporal evolutions of precipitating ice and cloud ice due to microphysical processes were studied using the microphysics-only model. Section 2 describes the methodology of the evaluation. Section 3 presents the results. Summary and discussion are given in Section 4.

2. Methodology

2a. Diagnosing detrainment of cloud condensate from a CRM

As explained in the *Glossary of Meteorology* of the American Meteorological Society (AMS 2000), “detrainment is the transfer of air from an organized air current to the surrounding atmosphere” and air current is “any moving stream of air”. Accordingly, we may define detrainment of cloud condensate from cumulus convection as “the transfer of cloud condensate from a cumulus cloud to the surrounding atmosphere”. Numerical cloud models have been used to study the dynamics of entrainment and detrainment because it has been difficult to obtain detailed knowledge of the dynamic and thermodynamic properties of clouds from observations. (e.g. Lin and Arakawa 1997; Carpenter et al. 1998 a, b, c; Cohen 2000). However, these studies contained little discussion about the detrainment of cloud condensate.

In reality, cloud and precipitating condensates are detrained from active convective regions (convective cores) to the relatively inactive convective regions, as well as from the inactive convective region to the non-convective (stratiform) region. The parameterized detrainment rate of cloud condensate in an SCM depends on *which rate is parameterized*: whether from active convective cores or from relatively inactive convective regions because properties of condensates and dynamical circulation vary with distance from convective cores. Likewise, in a CRM, the calculated detrainment rate depends on the partitioning between convective and stratiform regions (e.g., Tao et al. 1993).

About 99.9% of the surface precipitation in the SCM 29-day simulation was contributed by convective clouds through the convection parameterization. Precipitation by stratiform clouds through grid-scale cloud microphysical parameterization is negligible. This indicates that the SCM implicitly assumes that precipitation goes into the convective downdrafts, that is, no

precipitation is detrained. This assumption suggests that the SCM convective region includes both cores and inactive convective area. However, if we define the convective region in the CRM to be an area where detrainment of precipitation (graupel and rain) is zero as the SCM assumes, essentially no cloud ice (small ice crystals) or snow (large ice crystals that fall) would be detrained. The area of that convective region would not be negligible compared to that covered by stratiform clouds, which is inconsistent with the feature that the SCM does not consider the radiative impact of convective clouds. In other words, the SCM makes two assumptions that are inconsistent with each other: one is that convective region contains all of the precipitation; the other is that the radiative effect of convective clouds can be ignored. Therefore, it is difficult to make a meaningful comparison of detrainment rates of hydrometeors between the CRM and the SCM because of the difficulty of defining detrainment in the CRM that corresponds to what is envisioned in the SCM.

However, the SCM detrained cloud condensate (ice or water) is a source term in the predictive equation of cloud mixing ratio contained in stratiform clouds. This establishes a coupling between convective dymanics and radiation because the cloud fraction for radiation calculation is determined by cloud mixing ratio of stratiform clouds (Xu and Randall 1996). With a focus on clouds (rather than precipitation), we will compare the detrained cloud ice and snow in the CRM with detrained cloud ice in the SCM. As an effort to estimate the range of detrainment rates of cloud condensates in the CRM, two methods were used to define the convective regions. The method that represents detrainment from inactive convective regions is based on observations of the kinematic structures of mesoscale convective systems (Xu 1995). Using this method, convective regions consist of a convective “core” and two adjacent grid columns (one grid column is 2-km wide). A core consists of at least one convective grid column. The horizontal

distribution of the maximum cloud draft strength below the melting level ($|w_{max}|$) in a CRM grid column is used as the primary variable to find convective columns. A grid column is convective if it satisfies at least one of the following conditions: (a) $|w_{max}|$ is at least twice as large as the average over the four adjacent grid columns, (b) $|w_{max}|$ is greater than 3 m s^{-1}, (c) surface precipitation rate exceeds 25 mm h^{-1}. Results using this method are called *CRM_inact*. The method that represents detrainment from convective cores determines whether each grid point is part of a convective core. A grid point is part of a convective core if it satisfies two conditions: (a) the sum of cloud water and ice water mixing ratio is greater than 1% of the saturation water vapor mixing ratio, (b) vertical velocity is larger than 1 m s^{-1}. Results analyzed using this method are called *CRM_core*.

The detrainment of cloud condensate in the CRM can happen in two ways. One is that cloud condensate is transported by horizontal airflow out of a convective region. The other is the area of a convective region decreases so that part of cloud condensate previously contained in the convective region is left in non-convective region as part of non-convective clouds. The former process is more important than the latter in the CRM. CRM_inact and CRM_core are used to diagnose detrainment events in the 29-day simulation performed using the CRM for the ARM SGP site. A detailed comparison of detrainment of ice-phase cloud condensates between the SCM and the CRM will be presented in Section 3a. The detrainment is strongly associated with the sublimation in both models as will be shown in Section 3b.

2b. Description of 1-D microphysics model

The SCM assumes that detrainment occurs at a single-layer between two bounds at a time with only cloud ice or water. The detrained ice or water is sublimated/evaporated through microphysical parameterization, if the relative humidity (RH) is less than the critical value (RH_c), until RH reaches RH_c. The remained ice further decreases through conversion to snow due to depositional growth and aggregation of ice crystals and then through accretion by snowflakes. The SCM does not predict snow mixing ratio. It diagnoses snow flux at the bottom of each model layer assuming that the net production of snow by microphysical processes is balanced by the divergence of snow flux within one time step. In order to study the evolution of both precipitating ice (snow) and cloud ice formed by a detrainment event as what occurs in the SCM, we developed a 1-D microphysics-only model implemented with either the CRM or the SCM microphysical scheme to demonstrate the impact of the SCM assumption on the simulated snow field and to illustrate the differences between the CRM and SCM microphysical schemes.

The CRM and SCM use different one-moment bulk microphysical schemes. The microphysical scheme used in the CRM (Lin et al. 1983, Lord et al. 1984, Krueger et al. 1995) predicts the rates of change by various microphysical processes for mixing ratios of five species of hydrometeors: two non-precipitating (cloud water and cloud ice) and three precipitating (rain, snow, and graupel). The SCM microphysical scheme predicts the rate of change for mixing ratios of non-precipitating hydrometeors (cloud water and cloud ice) and diagnoses the fluxes of precipitating hydrometeors (rain and snow) (Zhao and Carr 1997). We designed two idealized simulations in which cloud ice is initially put at a saturated layer, with either the CRM or the SCM microphysical scheme. We call one “Dcrm” and the other “Dscm”. The process of ice sublimation is not activated in the two idealized simulations because cloud ice crystals do not fall out of the saturated layer.

Dcrm and Dscm start from initial profiles of temperature and moisture with initial cloud ice of 1.0 g kg^{-1} at a single saturated layer (390 to 370 mb) to represent the detrained cloud ice. The level of 0^oC temperature is located at ~ 760 mb. The model top is located at 310 mb and the model bottom is located at 850 mb. There are 27 layers and the vertical grid interval is 20 mb. No large-scale vertical velocity is imposed. The integration time is 4 hours. The time steps used are 10 seconds and 1800 seconds for Dcrm and Dscm, respectively, the same as those used for the 29-day simulations. The microphysical parameterizations in Dscm and Dcrm are addressed in more detail in the Appendix. Results frm Dcrm and Dscm will be presented in Section 3c.

3. Results

3a. Detrainment rates

As previously stated in the introduction, we used the large-scale forcing data at the ARM SGP site for the 29-day summer 1997 IOP to drive the CRM and the SCM. Detrainment events occur in the two simulations are represented in this section. The profiles of detrainment rate of non-precipitating cloud ice in the CRM and the SCM, averaged over the entire simulation period, are shown in Fig. 1a. Detrainment of cloud ice occur at heights between 4 and 14 km in both the SCM and the CRM simulations. The CRM profiles have their peaks of 0.005 and 0.033 g kg^{-1} hr^{-1} at 9-10 km (250 to 300 hPa). The SCM profile has a peak of 0.025 g kg^{-1} hr^{-1} located at ~ 8 km, about 1 km lower than the peaks of the CRM. The SCM values are between CRM_inact and CRM_core at heights above 8 km. However, at heights below 8 km, the SCM time-averaged detrainment rate is larger than those from the CRM. The excessively large detrainment rates of cloud ice in the SCM between 4 and 8 km contributed to its excessive sublimation rates of cloud ice, as will be shown in Section 3b.

The magnitude of detrainment rate of snow (not shown) is about the same as or a half of the magnitude of ice detrainment in CRM_inact and CRM_core, respectively. Fig. 1b is similar to Fig. 1a, except for the sum of the detrainment rates for cloud ice plus snow from the CRM. The peaks of the CRM profiles are 0.01 and 0.05 g kg^{-1} hr^{-1}, respectively. The CRM peaks are located at 9 to 10 km, the same height as the CRM detrainment of cloud ice. Compared to the CRM detrainment for both cloud ice and snow, the SCM detrained ice is between CRM_core and CRM_inact at heights above 7 km. However, it is greater than both CRM_core and CRM_inact below 7 km.

The time-height distributions of the hourly averaged detrainment rate of cloud ice in the SCM and of cloud ice plus snow in the CRM are displayed in Fig. 2. Only a 5-day subperiod starting at 2330 UTC 7 July is shown for illustration. However, the same features are found for the other periods. Note that the values represent averages over the CRM domain and the SCM grid box, respectively: they are the detrainment rates by cumulus ensembles. In reality, cumulus clouds at different stages of their evolution coexist in a grid box at a given time. These clouds have various sizes and top-heights so that detrainment occurs at the various heights within the cumulus ensemble. The distributions of hourly-averaged detrainment rates in the two models significantly differ from each other. Compared to the CRM, cloud ice is detrained at too thin a layer at a time and the detrainment occurs too sporadically in the SCM (Fig. 2a). CRM_inact (Fig. 2b) and CRM_core (Fig. 2c) time-height distributions show that detrainment of cloud ice and snow occurs over thicker layers at a time. The hourly detrainment rate of cloud ice diagnosed from CRM_inact and CRM_core (not shown) has a similar distribution to Fig. 2b and Fig. 2c, respectively. Detrainment lasts longer in CRM_core than in CRM_inact because detrainment from cores starts earlier than detrainment from an inactive convective region and, as convective activities decay,

detrainment from an inactive convective region may stop earlier than detrainment from convective cores.

The time averaged detrainment rates (Fig. 1) depend on instantaneous detrainment rates and occurrence frequency of detrainment events. The occurrence frequency at a level is the fraction of time when a detrainment event occurs in the simulations. Detrainment events occur too infrequently in the SCM compared to those in the CRM (Fig. 3). The 29-day averaged occurrence frequency of detrainment in the SCM (solid line in Fig. 3a) is <~ 0.02 at all heights with a peak at 9 km. The two profiles of cloud ice detrainment for the CRM (dashed lines in Fig. 3a) have a peak of 0.15 (CRM_inact) and 0.44 (CRM_core), respectively, located at 10 km. When snow is included, the occurrence frequency of detrainment increases at heights below 10 km for CRM_inact (Fig. 3b) and below 5 km for CRM_core (Fig. 3c). This suggests that a few detrainment events have snow detrained without ice in the CRM. Compared to CRM_inact, CRM_core has a greater occurrence frequency at heights above 5 km but a smaller one below.

We have shown that, the magnitude of the SCM detrainment rate of cloud ice is somewhere between CRM_inact and CRM_core detrainment rates of cloud ice plus snow at heights above 7 km and greater than both CRM_core and CRM_inact below 7 km (Fig. 1). This, combined with the fact that fewer detrainment events occur in the SCM (Fig. 3), indicates that the instantaneous detrainment rate is too large for the SCM. This is demonstrated by the 2-D histograms of instantaneous detrainment rate (Fig. 4). The 2-D histogram is the number of detrainment events in a bin of 0.25 g kg^{-1} hr^{-1} at each model level divided by the total number of detrainment events at all levels over the entire range of detrainment rate. The SCM mode is located at the bin of 0.5 to 0.75 g kg^{-1} hr^{-1} and the height of 11 to 12 km. The detrainment rate tends to increase with decreasing height and can be as large as 3 g kg^{-1} hr^{-1} at heights between 5 to

9 km (Fig. 4a). The 2-D histograms of detrainment rate for cloud ice plus snow diagnosed from CRM_inact (Fig. 4b) and CRM_core (Fig. 4c) appear to be similar to each other, but significantly different from the SCM. Both CRM_inact and CRM_core have a mode at the smallest bin of detrainment rate. The maximum detrainment rate is ~ 1.35 g kg^{-1} hr^{-1} for CRM_core and ~ 0.76 g kg^{-1} hr^{-1} for CRM_inact, smaller than the SCM's (4.44 g kg^{-1} hr^{-1}).

The fact that the SCM detrains in a layer that is too thin at a time with an instantaneous rate that is too large, combined with the assumptions that *in-cloud* stratiform cloud ice mixing ratio is horizontally homogeneous within the SCM grid and that snow is not part of clouds, can partly explain our findings in Part I; that is 1) too many cirrus layers occur at a single model level when snow is not included as part of the cirrus clouds, 2) the layer-mean IWC and IWP distributions of the cirrus are more skewed toward larger values than observed, and 3) the layer-mean IWC decreases with increasing physical thickness in contrast to the observations and the CRM results. If detrainment occurred over thicker layers, the clouds would be physically thicker for the same IWP. This would decrease the IWC values for the detrainment-formed clouds. If detrainment lasted longer with the same total IWP, clouds would have smaller IWP and IWC at a time. Both situations would tend to alleviate the deficiencies of the SCM simulations of cirrus clouds.

3b. Sublimation of cloud ice and snow

We have shown that, compared to the CRM, too much cloud ice is detrained in the SCM at too thin a layer at a time. How would the detrainment events influence the sublimation process in the SCM and the CRM? Large-scale sublimation of cloud ice in the SCM is determined following Sundqvist et al. (1989). Cloud ice sublimation occurs only where the relative himudity is less than

the critical value (RH_c). The SCM assumes that all water vapor from evaporation is used to increase the relative humidity until RH_c is reached. Based on Clausius-Clapeyron equation and the first law of thermodynamics, increase of water vapor mixing ratio (q_v) due to ice sublmation can be expressed by

$$ISUB = \frac{q_{vs} - q_v}{1 + q_{vs}\dfrac{L_s^2}{C_p R_v T^2}} \quad (1)$$

where q_{vs} is the saturation water vapor mixing ratio, L_s is the latent heat of sublimation, C_p is the specific heat at constant pressure, R_v is the gas constant for water vapor. The SCM calculates the amount of sublimated cloud ice in one time step using (1) with q_{vs} multiplied by RH_c. Ice sublimation rate in the CRM is determined by the saturation adjustment scheme of Lord et al. (1984). Determination of snow sublimation in the SCM and CRM, respectively, is described in the Appendix.

We analyzed the sublimation rates of cloud ice and snow, respectively, using results from the same 29-day simulations as those used to analyze detrainment of cloud condensate in Section 3a. To determine the 29-day time-averaged sublimation rate for cloud ice and snow, respectively, instantaneous rates sampled at 5-min interval from the CRM and every time step (30-min) from the SCM are used. The profiles of the time-averaged sublimation rates are compared between the CRM and SCM simulations (Fig. 5). Cloud ice sublimation occurs in atmospheric layers located between 4 and 14 km in both simulations (Fig. 5a). However, too much cloud ice is sublimated in the SCM in all layers where ice sublimation occurs, especially in the layers below 8 km where too much cloud ice detrainment occurs (Fig. 1a). The overestimation of cloud ice sublimation in the

SCM could contribute to its excessively moist atmosphere (Figs. 1 and 2 in part I show that the SCM had too warm atmosphere and an overestimation of relative humidity, respectively.).

Snow sublimation occurs at heights between 3 and 12 km in the SCM and between 3 and 10 km in the CRM (Fig. 5b). The time-averaged rate of snow sublimation is greater in the CRM than the SCM at heights below 9km, especially near freezing level where the SCM's rate is negligible. Comparing Fig. 5a with Fig. 5b, one can see that the snow sublimation rate is about 40% of the ice sublimation rate in the SCM, opposite to the CRM which has a snow sublimation rate being about 3 times of the ice sublimation rate. When the sublimation rate of cloud ice plus snow is compared (Fig. 5c), the SCM has a greater rate than the CRM at all heights except near the freezing level.

We computed the occurrence frequency of sublimation events at a level as the fraction of time when instantaneous sublimation rate is greater than 10^{-3} g kg^{-1} hr^{-1}. The time-averaged occurrence frequency of sublimation events for cloud ice and snow, respectively, are compared between the CRM and SCM (Fig. 6). In spite of its greater sublimation rate of cloud ice averaged over the simulation period (Fig. 5a), ice sublimation occurs too infrequently in the SCM (the time-average occurrence frequency < 0.1 at all levels) compared to the CRM. The occurrence frequency of ice sublimation in the SCM varies little with height, as opposite to the CRM's profile which has a peak of 0.42 at 10 km and decreases rapidly upward and downward. The SCM occurrence frequency of snow sublimation events has a peak of 0.25 at 7 km (solid line in Fig. 6b), ~ 1 km lower than the peak of the CRM. Compared to the SCM, sublimation of snow occurs more frequently in the CRM at heights below 10 km.

The time-height distributions of hourly cloud ice sublimation rate are significantly different in the CRM and SCM simulations (Fig. 7a and 7b). Results during 5 days starting at July

7 23:30 UTC are provided for illustration, but similar features are found during the other periods, too. The cloud ice sublimation in the SCM simulation has a similar distribution (Fig. 7a) to that of its detrainment (Fig. 2a). A large amount of cloud ice is sublimated when detrainment occurs. The sublimation occurs at a single layer at a time and lasts for only a short period of time with generally larger rates than the CRM's. The CRM sublimation of cloud ice appears to occur more smoothly in both height and time than the SCM. Figures 2 and 7 suggest that cloud ice sublimation is strongly associated with cloud ice detrainment in the SCM and CRM and, therefore, indicate that greater cloud ice sublimation in the SCM may be due to its greater detrainment rate of cloud ice. This is confirmed by the 2-D histograms of instantaneous rates of cloud ice sublimation (Fig. 8).

We calculated the probability density of ice sublimation rate occurred at each layer of the SCM and CRM, respectively. The ice sublimation events are grouped into two categories: in one category the sublimation events are not accompanied by occurrence of cloud ice detrainment at the same time and level; in the other category they are. For each category, the probability density in a certain bin at a level is the number of ice sublimation events within the bin at the level normalized by the total number of events at all levels. The bin width is 0.25 g kg^{-1} hr^{-1} for the SCM and 0.01 g kg^{-1} hr^{-1} for the CRM. The results are represented in Figs. 8a and 8b for the SCM and Figs. 8c and 8d for the CRM. Note that difference scales of coordinate are used for better illustration. When occurrence of an ice sublimation event is not accompanied by a detrainment event, the SCM cloud ice sublimates at a rate < ~ 0.3 g kg^{-1} hr^{-1} at any height. When sublimation events are accompanied by detrainment events, significantly larger (by a factor of 10) sublimation rates occur. Similar to the 2-D histograms of ice detrainment rate in the SCM (Fig. 4a), there is a tendency for the rate of sublimation (when accompanied by a detrainment event; Fig. 8c) to

increase with decreasing height. The CRM's 2-D histograms of cloud ice sublimation rate (Figs. 8c and 8d) appear similar to each other. The CRM ice crystals sublimate at domain-averaged rates < ~ 0.06 g kg^{-1} hr^{-1}, no matter if detrainment occurs at the same time or not. The modes are located at the smallest bin of sublimation rate. The sublimation rates accompanied by detrainment (Fig. 8d) are only slightly greater than the rates that are not accompanied by detrainment events (Fig. 8b).

For snow sublimation rate, we determined the 2-D histograms using a bin width of 0.025 g kg^{-1} hr^{-1} for the SCM and CRM simulations (Figs. 8e and 8f). Both the SCM and CRM have a mode located at the smallest bin. The height of the mode is ~ 7 km in the SCM, lower than the CRM's (~ 9 km). The typical magnitudes of snow sublimation rates are comparable between the SCM and CRM. Therefore, the greater time-averaged snow sublimation rate in the CRM (Fig. 7b) is mainly due to more frequent occurrences of snow sublimation.

We conclude that, compared to the CRM simulation, detrained ice crystals sublimate at excessively large instantaneous rates in the SCM. This results in too large time-averaged sublimation rate of cloud ice, although detrainment occurs more infrequently in the SCM. The reasons are too much cloud ice is detrained and the detrained ice is allowed to sublimate until the grid-mean relative humidity reaches the critical value using (1) with q_{vs} multiplied by RH_c. This assumption is probably invalid for detrained ice. When detrainment occurs in reality, ice is detrained along with a volume of saturated air. Turbulent mixing would occur at the boundaries of the detrained air resulting in subsaturation and, hence, the detrained ice may sublimate. However, sublimation is probably not efficient at the inner part of the detrained air and the grid-mean relative humidity would not reach the critical value every time detrainment occurs. Since the partitioning between cloud ice and snow differs between the SCM and CRM, a comparison of the

sublimation rate for cloud ice plus snow appears to be more appropriate. However, the time-averaged sublimation rate of cloud ice plus snow differs significantly between the two simulations with the SCM's being larger.

3c. Results from the idealized 1-D simulations

As described previously in Section 2b, we use a 1-D microphysics-only model to evaluate the SCM's assumption that net production of snow by microphysical processes is balanced by the divergence of snow flux in one time step. Results from two idealized simulations are represented in this section. In the idealized simulations, cloud ice is initially put at a saturated layer. Evolution of cloud ice and snow is determined by either the CRM or the SCM's microphysics parameterization.

Fig. 9 shows the profiles of F_s at 0.5, 1.0, 1.5, and 2.0 hr in Dscm (Fig. 9a) and Dcrm (Fig. 9b) simulations. It is obvious that F_s in Dscm extends to lower layers compared to that in the Dcrm. Consequently, the snow mixing ratio diagnosed from the Dscm F_s extends too low compared to the Dcrm predicted (not shown). The results explain why the SCM cirrus layers are too thick and have too low base-heights *when snow is included as a part of cirrus* as found in Part I.

With only microphysical processes included, the prognostic equation for snow mixing ratio is

$$\frac{\partial}{\partial t} q_s = S_{micro} + \frac{1}{\rho} \frac{\partial}{\partial z} \rho q_s V_s \qquad (2)$$

where S_{micro} is the net production of snow by microphysical processes. During transient (adjustment) period, signal travels downward at speed V_g (positive downward). In a model with time step Δt and grid interval Δz, the Courant-Friedrichs-Lewy (CFL) stability criterion is $V_g \Delta t < \Delta z$, or $V_g < \frac{\Delta z}{\Delta t}$. However, for the SCM, we have $\frac{\Delta z}{\Delta t} \approx 1$ m s^{-1}. Thus, CFL will not be satisfied if $V_g \geq 1$ m s^{-1}, as it is for rain. For snow, it may be satisfied. Using an implicit method can remove this restriction, however.

In the SCM, it is assumed that

$$S_{micro} = -\frac{1}{\rho}\frac{\partial}{\partial z}\rho q_s V_s \ . \tag{3}$$

This assumption ignores the transient state. The basis for this assumption is that sedimentation adjusts quickly (relative to variation of S_{micro} and within one time step) to an approximately steady state. The adjustment time scale is $\tau \sim \frac{H}{V_g}$ where H is the thickness of precipitation layer. For snow, $H \sim 8$ km, $V_g \sim 1$ m s^{-1}, so $\tau \sim 8000$ s. For rain, $H \sim 4$ km, $V_g \sim 5$ m s^{-1}, so $\tau \sim 1000$ s. Therefore, the assumption is not satisfied for snow and results in snow flux extending too low. However, it is better for rain because of its larger fall speed and thinner falling layer.

We have demonstrated that snow flux extends too low in the Dscm simulation (Fig. 9), due to the balance assumption used (Eq. 3). This caused sublimation of snow to occur at layers below ~ 600 hPa in Dscm because snow sublimation rate depends on snow flux in Dscm (A3). This results in an overestimation of downward transport of water vapor through snow sublimation. The excessive moistening is demonstrated by the change of relative humidity from its initial value (Fig. 10) in the two simulations. Relative humidity increases with time due to snow sublimation. While it extends to lower heights in Dscm, the increase of RH occurs at layers above ~ 600 hPa in

Dcrm because snow did not fall to layers below. In the 29-day simulations with the full physics, the SCM snow sublimation tends to occur at lower heights than the CRM (Figs. 8e and 8f), consistent with the idealized simulations. However, the time-averaged sublimation rate of snow is greater in the CRM at heights below 9 km (Fig. 5b) because of more frequent occurrence (Fig. 6).

In the saturated layer, cloud ice decreased from initial value (1.0 g kg^{-1}) due to conversion to snow by various microphysical processes. The amount of cloud ice mixing ratio in the saturated layer decreases to 0.62 and 0.26 g kg^{-1} at 0.5 hr in Dscm and Dcrm, respectively (Table 1). This suggests that, although the total amount of snow converted from ice in Dscm is less than that in Dcrm during the entire simulation period, the balance assumption of snow used in Dscm caused its snow flux to extend too low.

We examined the relative contribution of individual microphysical process that converted ice to snow. For Dscm, the only process activated is depositional growth and aggregation of ice crystals (SAUT). Accretion of ice by snowflakes (SACI) is not activated because no snow falling from above: $F_s = 0$ in Eq. (A2). Both SAUT and SACI, as well as transformation of cloud ice to snow via the growth of Bergeron-process embryos (SFI), are activated in Dcrm. These rates, averaged over half of an hour, are presented in Table 2 for the first two and half hours. The Dscm SAUT rates are 0.77, 0.47, 0.29, 0.18, 0.11 g kg^{-1} hr^{-1}, respectively. The net rates by all microphysical processes in Dcrm are 1.49, 0.28, 0.12, 0.06, and 0.03 g kg^{-1} hr^{-1}. Therefore, Dcrm ice is converted to snow at about twice of the conversion rate of Dscm for the first half hour. However, during the later four half-hours Dcrm net conversion rate is about 0.60, 0.41, 0.33, and 0.27, respectively, of that in Dscm. In Dcrm, the relative contribution of various microphysical processes varied with time. The SAUT contributed to 50% of the net rate for the first half hour

and then was inactivated because ice mixing ratio decreased to 0.26 g kg^{-1}, less than the threshold value (q_{i0}) in (A1). The SACI contributed to 8% and 4% of the net rate during the first two half-hours, respectively, and then became zero. Contribution from SFI is 42% for the first half-hour, 96% for 0.5 - 1.0 hr, and then 100% afterwards.

It should be noted that, even if the SCM used the same microphysical scheme as in the CRM, results from a full physics simulation would not be the same as in the CRM. The differences between the CRM and SCM would result not only from differences in parameterizations of other physical processes, but also from the inputs to the microphysical parameterization with different spatial and temporal scales.

4. Summary and discussion

Kilometer-scale cirrus statistics were produced using results from a 29-day simulation of the ARM SGP summer 1997 IOP performed by an SCM based upon the NCEP GFS model in Part I of this series of study (Luo et al. 2005). The present study has investigated why the composite characteristics of the SCM-simulated cirrus clouds are significantly different from the cloud radar observations and CRM simulation described in Part I. We compared results from the SCM and CRM simulations in this study. We have shown that the reasons are related to the parameterizations of detrainment from deep convection and ice-phase microphysical processes in stratiform clouds in the SCM.

The detrainment process as represented in the SCM was evaluated through a comparison between the 29-day simulations performed by the SCM and the CRM for the summer 1997 IOP at the ARM SGP site. The time-averaged detrainment rate of cloud ice simulated by the SCM was bounced by the two rates (core and inactive convection) diagnosed from the CRM simulation at

heights above 7 km, but it was larger than both of the CRM's below 7 km. The SCM had much larger instantaneous values of detrainment rate for cloud ice. The detrainment events occurred less frequently and at a single model level at a time. This contributes to a large occurrence frequency of physically thin cirrus cloud layers, when snow is not included as a part of cirrus clouds as the SCM does. Combined with the SCM's assumptions that in-cloud ice mixing ratio is horizontally homogeneous and that snow is not a part of clouds, this may explain why the distributions of the kilometer-scale IWP and the layer-mean IWC of cirrus clouds are excessively skewed towards large values, and that the layer-mean IWCs decrease with increasing cloud physical thickness found in Part I. Even though the time-averaged detrainment rate of cloud ice were about right, the combination of infrequent occurrences of detrainment with the assumptions of horizontal homogeneity of in-cloud ice mixing ratio and that clouds do not include snow would not allow the SCM to produce realistic kilometer-scale statistics of cirrus properties. Inclusion of multiple cumulus cloud types as in the original Arakawa-Schubert scheme so that detrainment of cloud ice will happen over multiple layers, or detrain into a thicker layer (not at a single layer only) is expected to help. Another possible remedy for the large-scale model is to use a higher horizontal resolution so that more possible detrainment levels will be sampled.

Characterisitcs of cloud ice sublimation are strongly associated with the features of cloud ice detrainment occurred in the SCM. In the 29-day simulation, the SCM cloud ice sublimates immediately after being detrained at excessively large rates, compared to the CRM. One reason is that too much cloud ice is detrained. Another reason is that the detrained ice is allowed to sublimate until the grid-mean relative humidity reaches the critical value. Although too few cloud ice sublimation events occurred in the SCM, the excessively large instantaneous rates resulted in a larger 29-day averaged ice sublimation rate than the CRM. This contributed to the excessively

moist atmosphere in the SCM found in Part I. One may solve this problem by prognostically determining cloud fraction as proposed by Tiedtke (1993). Then, the detrained ice simply increases the cloud fraction according to the volume of detrained air, and cloud ice sublimates at cloud boundaries by turbulent mixing of cloud air and unsaturated environmental air.

The SCM diagnoses the snow flux assuming that the net generation by microphysical processes is balanced by the net divergence of snow flux in one time step. This assumption is satisfied only if the adjustment time of snow sedimentation is less than the time step, which is not true for the SCM. As demonstrated by the 1-D idealized microphysics-only simulations, use of this assumption results in snow extending too low. This, combined with the SCM assumption that snow and cloud ice are horizontally homogeneous, may explain the findings presented in Part I that, when snow is included as a part of cirrus clouds, the SCM cirrus layers are too thick and their base heights are too low. Prognostically determining the snow mixing ratio should be able to alleviate this problem. If the diagnostic approach is kept, use of a smaller SCM time step will worsen the problem because the assumption for the diagnostic approach is less likely to be satisfied.

This study has demonstrated how CRMs complement observations for the evaluation of SCMs. It would be interesting to modify the SCM with, for example, a detrainment parameterization with multiple detrainment layers, a prognostic snow equation or a prognostic cloud fraction, and test the impacts of the modifications on the NCEP GFS SCM simulated clouds. However, such work is not included and could be a meaningful extension of the present study. The NCEP GFS SCM is used as an example to demonstrate our evaluation method, which is a very important step towards improving models.

Acknowledgements. This research was supported by the Environmental Sciences Division of the U.S. Department of Energy (DOE) as part of the Atmospheric Radiation Measurement program, under Grant DEFG03-94ER61769 (Luo and Krueger) and by NASA EOS Interdisciplinary study program (Xu). Suggestions from two anonymous reviewers are greatly appreciated. We thank Drs. Zachary A. Eitzen of NASA Langley Research Center and Shaocheng Xie of Lawrence Livermore National Laboratory for improving an earlier version of this paper.

APPENDIX

In the Dscm simulation, the method to determine snow flux and the ice-phase microphysics used in the NCEP SCM (Zhao and Carr 1997) are used. Dscm simulation does not predict the snow mixing ratio. It diagnoses the snow flux (F_s) at the bottom of each model layer: F_s is the vertical integral of the net snow production by microphysical processes at/above that layer. The microphysical processes for snow production in Dscm simulation are the aggregation of ice crystals (SAUT), the accretion of ice crystals by snow (SACI), and the microphysical process for snow sink are the sublimation (SSUB) and melting (SMEL). These terms are determined following Zhao and Carr (1997) but using different values for some parameters included in the formulations.

The snow production caused by the size increase of cloud ice particles due to depositional growth and aggregation of small ice crystals is expressed by

$$SAUT = a(q_i - q_{i0}) \tag{A1}$$

where $a = 5 \times 10^{-4} \times \exp(0.025 T_c)$ s^{-1} (T_c is temperature in ^{o}C), and $q_{i0} = 10^{-5} p$ g kg^{-1} (p is pressure in hPa). The coefficient a is a half of that in Zhao and Carr (1997; Eq. 26). The threshold of cloud ice mixing ratio for this process to activate (q_{i0}) decreases linearly with decreasing pressure in the SCM and is smaller than the constant (0.1 g kg^{-1}) used by Zhao and Carr (1997).

The accretion of ice by snowflakes is an aggregation process and calculated in the SCM using

$$SACI = c_s q_i F_s \tag{A2}$$

where the collection coefficient c_s is that of Zhao and Carr (1997; Eq. 29) multiplied by $\frac{800}{\Delta t}$ where Δt is the time step interval.

In the SCM, snow is allowed to sublimate at points with relative humidity with respect to ice less than the critical value RH_c (Zhao and Carr 1997; Eq. 36) and with temperature $T < 0\ ^oC$. The sublimation rate of snow (SSUB) is computed using

$$SSUB = (c_1 + c_2 T_c)\frac{RH_c - RH}{RH_c} F_s \tag{A3}$$

where $c_1 = 0.004\ m^2\ kg^{-1}$, $c_2 = 5.336x10^{-7}\ m^2\ kg^{-1}\ K^{-1}$, and RH_c is 0.85. Both c_1 and c_2 in the SCM microphysics scheme are those used by Zhao and Carr (1997) modified by a factor of $\frac{800}{\Delta t}$, respectively.

The SCM microphysics scheme includes snow melting below the freezing level in two ways, following Zhao and Carr (1997). One is the continuous melting of snow due to the increase in temperature as snow falls through the $T=0^oC$ level. The other is the immediate melting of snow by collection of the cloud water below the $T=0^oC$ level. The first melting process is parameterized as a function of temperature and snow fall flux. The second melting process, resulting from the interaction between melting snow and cloud water below the freezing level, did not occur in Dscm due to lack of cloud water.

Snow flux at each model level $F_s(p)$ (p is pressure) can be expressed by

$$F_s(p) = \frac{1}{g}\int_{p_t}^{p}(SAUT + SACI - SSUB - SMEL)\,dp \tag{A4}$$

p_t is pressure at the top of model. Some terms (SACI, SSUB, and SMEL) on the right-hand side of (A4) are functions of F_s. These terms at each level are computed first using the F_s from the level above. Then all terms at this level are added to the F_s from the level above to give F_s for the next level calculation. This procedure is done level by level downward from cloud top following Zhao and Carr (1997).

The CRM uses Lin scheme (Lin et al 1983) to determine microphysical rates of water species. In the Dcrm simulation, the source terms in the predictive equation of snow include three microphysical processes: the depositional growth and aggregation of ice crystals (SAUT), the accretion of ice crystals by snow (SACI), and the transformation of cloud ice to snow via the growth of Bergeron-process embryos (SFI) as well as convergence of snow flux, while the sink terms of snow are the sublimation (SSUB) and divergence of snow flux.

The CRM uses the same formula as (A1) to determine the conversion rate of ice to snow due to depositional growth and aggregation of ice crystals. However, the CRM uses different values for a and q_{i0}: $a = 0.1 \times \exp(0.025 T_c)$ s^{-1}, and $q_{i0} = 0.6$ g kg^{-1}. This indicates that activation of this process requires a larger amount of q_i in the CRM than the SCM. Snow growth rate through accretion of ice (SACI) is based on the geometric sweep-out concept integrated over all snow sizes for the assumed exponential size distribution of snowflakes. The CRM determines SFI using $SFI = \frac{q_i}{\Delta t}$, where Δt is the temperature-dependent timescale for an ice crystal to grow from 40 to 100 μm. This process is ignored in the SCM.

The Lin scheme allows snow sublimation to occur when temperature $T < 0\ ^{o}C$ and if the air is subsaturated with respect to ice. Snow sublimation rate is based on the depositional growth of snow crystals given by Byers (1965) with a modified ventilation effect (Lin et al. 1983). Snow

melts if the temperature (T) is above 0^{o}C. However, it did not occur in Dcrm because snow never reached the T=0^{o}C level in this particular simulation.

References

American Meteorological Society, 2000: The Glossary of Meteorology. Approx. 850 pp.

Arakawa, A. and W. H. Schubert, 1974: Interaction of a cumulus ensemble with the large-scale environment, Part I. *J. Atmos. Sci.*, **31**, 674-704.

Byers, H. R., 1965: *Elements of Cloud Physics*. The University of Chicago Press, 191 pp.

Carpenter, R. L., K. K. Droegemeier, A. M. Blyth, 1998a: Entrainment and Detrainment in Numerically Simulated Cumulus Congestus Clouds. Part I: General Results. *J. Atmos. Sci.*, **55**, 3417-3432.

--, --, and --, 1998b: Entrainment and Detrainment in Numerically Simulated Cumulus Congestus Clouds. Part II: Cloud Budgets. *J. Atmos. Sci.*, **55**, 3433-3439.

--, --, and --, 1998c: Entrainment and Detrainment in Numerically Simulated Cumulus Congestus Clouds. Part III: Parcel Analysis.*J. Atmos. Sci.*, **55**, 3440-3455.

Cohen, C., 2000: A quantitative investigation of entrainment and detrainment in numerically simulated cumulonimbus clouds. *J. Atmos. Sci.*, **57**, 1657-1674.

Del Genio, A. D., M.-S. Yao, W. Kovari, and K.-W. Lo, 1996: A prognostic cloud water parameterization for global climate models. *J. Climate*, **9**, 270-304.

Dong, X., and G. G. Mace, 2003: Profiles of low-level stratus cloud microphysics deduced from ground-based measurements. *Journal of Atmospheric and Oceanic Technology.* 20, 42-53.

Fowler, L. D., D. A. Randall, and S. A. Rutledge, 1996: Liquid and ice cloud microphysics in the CSU General Circulation Model. Part I: Model description and simulated microphysical processes. *J. Climate.*, **9**, 489-529.

Heymsfield, A., and J. Iaquinta, 2000: Cirrus crystal terminal velocities. *J. Atmos. Sci.*, **57**, 916-938.

IPCC, 2001: Intergovernmental Panel on Climate Change, *Climate Change 2001*, Third Assessment Report of the IPCC. The Scientific Basis. A contribution of working Group I. Cambridge University Press.

Krueger, S. K., 1988: Numerical simulation of tropical cumulus clouds and their interaction with the subcloud layer. *J. Atmos. Sci.*, **45**, 2221-2250.

--, Q. Fu, K. N. Liou, and H.-N. S. Chin, 1995: Improvements of an ice-phase microphysics parameterization for use in numerical simulations of tropical convection. *J. Appl. Meteor.*, **34**, 281-287.

--, and Y. Luo, 2005: Cloud properties simulated by a Single-Column Model. Part III: Cloud type radiative forcing and comparison with satellite observations and results from a CRM. To be submitted.

Lin, C. and A. Arakawa, 1997: The macroscopic entrainment processes of simulated cumulus ensemble. Part II: Testing the entrainment plume model. *J. Atmos. Sci.*, **54**, 1044-1053.

Lin, Y. L., R. D. Farley, and H. D. Orville, 1983: Bulk parameterization of the snow field in a cloud model. *J. Climate Appl. Meteor.*, **22**, 1065-1092.

Lord, S. J., H. E. Willoughby and J. M. Piotrowicz, 1984: Role of a parameterized ice-phase microphysics in an axisymmetric tropical cyclone model. *J. Atmos. Sci.*, **41**, 2836-2848.

Luo, Y., S. K. Krueger, G. G. Mace, and K.-M. Xu, 2003: Cirrus cloud statistics from a cloud-resolving model simulation compared to cloud radar observations. *J. Atmos. Sci.*, **60**, 510-525.

--, --, and S. Moorthi, 2005: Cloud properties simulated a single-column model. Part I: Comparison to cloud radar observations of cirrus clouds. *J. Atmos. Sci.*, in press.

Mace, G. G., E. E. Clothiaux, and T. P. Ackerman, 2001: The composite characteristics of cirrus clouds; bulk properties revealed by one year of continuous cloud radar data. *J. Climate*, **14**, 2185-2203.

Ose, T., 1993: An examination of the effects of explicit cloud water in the UCLA GCM. *J. Meteor. Soc. Japan*, **71**, 93-109.

Pan, H.-L., and W.-S. Wu, 1995: Implementing a mass flux convection parameterization package for the NMC medium-range forecast model. National Meteorological Center, Office

Note 409, 40 pp. [Available from NCEP/EMC, 5200 Auth Road, Camp Springs MD 20746]

Randall, D. A., K.-M. Xu, R. J. C. Somerville, and S. Iacobellis, 1996: Single-column models and cloud ensemble models as links between observations and climate models. *J. Climate.*, **9**, 1683-1697.

--, and co-authors, 2003: Confronting models with data. *Bull. Amer. Meteor. Soc.*, **84**, 455-469.

Rossow, W. B., and R. A. Schiffer, 1991: ISCCP cloud data products. *Bull. Amer. Meteor. Soc.*, **72**, 2-20.

--, A. W. Walker, D. Beuschel, and M. Roiter, 1996: International Satellite Cloud Climatology Project (ISCCP) description of new cloud datasets. WMO/TD 737, World Climate Research Programme (ICSU and WMO), 115 pp.

Stokes, G. M., and S. E. Schwartz, 1994: The Atmospheric Radiation Measurement (ARM) Program: Programmatic background and design of the Cloud and Radiation Test bed. *Bull. Amteor. Soc.*, **75**, 1201-1221.

Tao, W.-K., J. Simpson, C.-H. Sui, B. Ferrier, S. Lang, J. Scala, M.-D. Chou, and K. Pickering, 1993: Heating, moisture, and water budgets of tropical and midlatitude squall lines: comparisons and sensitivity to longwave radiation. *J. Atmos. Sci.*, **50**, 673-690.

Tiedtke, M., 1993: Representation of clouds in large-scale models. *Mon. Wea. Rev.*, **121**, 3040-3061.

Wielicki, B. A., B. R. Barkstrom, E. F. Harrison, R. B. Lee III, G. L. Smith, and J. E. Cooper, 1996: Clouds and the Earth's Radiant Energy System (CERES): An Earth Observing System Experiment. *Bull. Amer. Meteor. Soc.*, **77**, 853-868.

Xu, K.-M., 1995: Partitioning mass, heat, and moisture budgets of explicitly simulated cumulus ensembles into convective and stratiform components. *J. Atmos. Sci.*, **52**, 551-573.

--, and D. A. Randall, 1996: A semiempirical cloudiness parameterization for use in climate models. *J. Atmos. Sci.*, **53**, 3084-3102.

Zhang, M. H., and J. L. Lin, 1997: Constrained variational analysis of sounding data based on column-integrated budgets of mass, heat, moisture, and momentum: approach and application to ARM measurements. *J. Atmos. Sci.*, **54**, 1503-1524.

--, --, R. T. Cederwall, J. J. Yio, and S. C. Xie, 2001: Objective analysis of ARM IOP data: method and sensitivity. *Mon. Wea. Rev.*, **129**, 295-311.

Zhao, Q., and F. H. Carr, 1997: A prognostic cloud scheme for operational NWP models. *Mon. Wea. Rev.*, **125**, 1931-1953.

TABLE 1. Cloud ice mixing ratio (g kg^{-1}) at the saturated layer in the first two hours of Dscm and Dcrm.

Time (hr)	0.0	0.5	1.0	1.5	2.0
Dscm	1.00	0.62	0.38	0.23	0.15
Dcrm	1.00	0.26	0.12	0.05	0.02

TABLE 2. Half-hourly averaged decreasing rates of cloud ice mixing ratio (g kg^{-1} hr^{-1}) at the saturated layer in the first two and half hours of Dscm and Dcrm by various microphysical processes.

	0.0 - 0.5 hr	0.5 - 1.0 hr	1.0 - 1.5 hr	1.5 - 2.0 hr	2.0 - 2.5 hr
Dscm (SAUT)	0.77	0.47	0.29	0.18	0.11
Dcrm (net rate by microphs.)	1.49	0.28	0.12	0.06	0.03
Dcrm (SAUT)	0.74	0.00	0.00	0.00	0.00
Dcrm (SACI)	0.12	0.02	0.00	0.00	0.00
Dcrm (SFI)	0.62	0.27	0.12	0.06	0.03

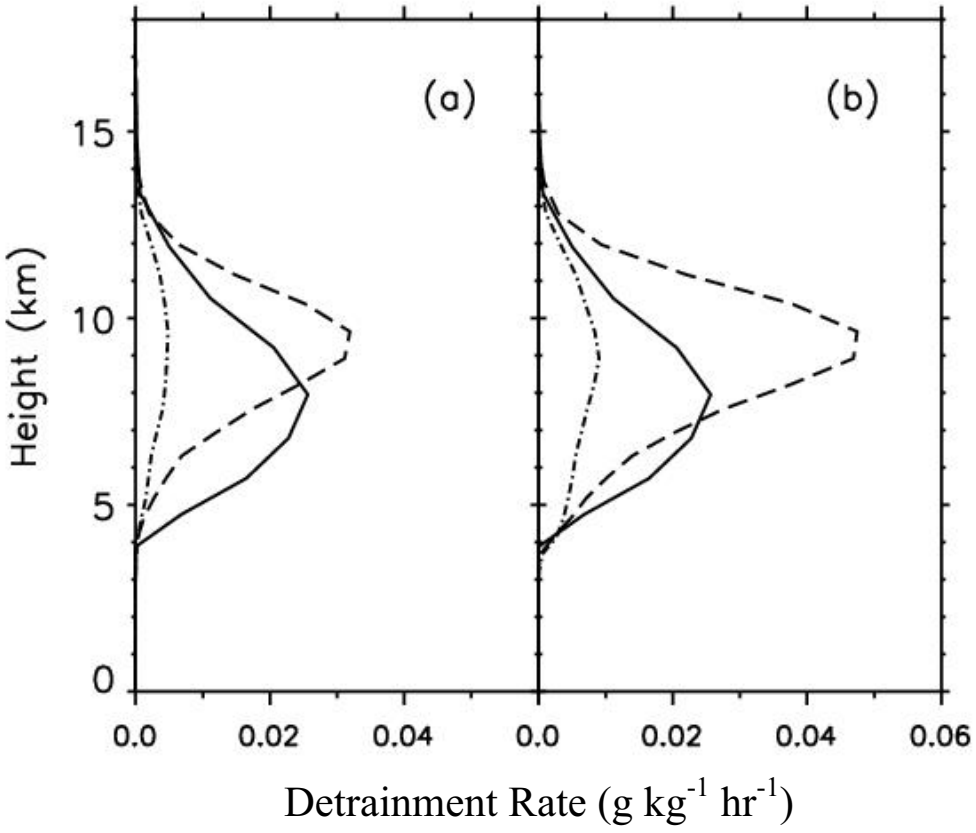

Figure 1. (a) The profiles of detrainment rate (g kg^{-1} hr^{-1}) of cloud ice averaged over the entire simulation period for the SCM (solid line), CRM_inact (dot-dashed line), and CRM_core (dashed line). (b) Similar to (a), except that the detrainment of cloud ice plus snow for CRM_inact (dot-dashed line) and CRM_core (dashed line) are shown.

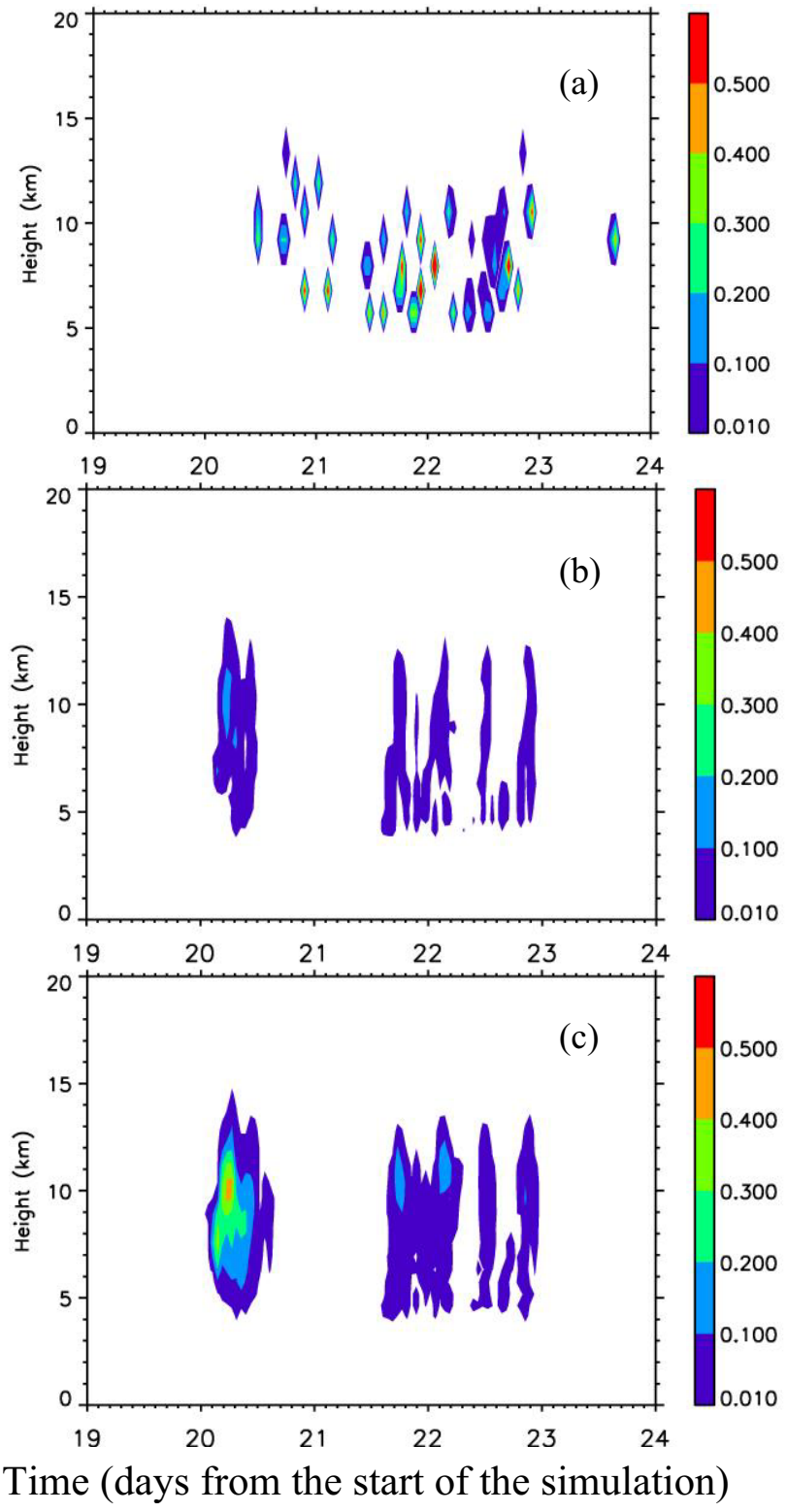

Figure 2. The time-height distribution of hourly averaged detrainment rate of cloud ice in the SCM (a), and hourly averaged detrainment rate of cloud ice plus snow in CRM_inact (b), and CRM_core (c), respectively. The detrainment rates are in g kg^{-1} hr^{-1}.

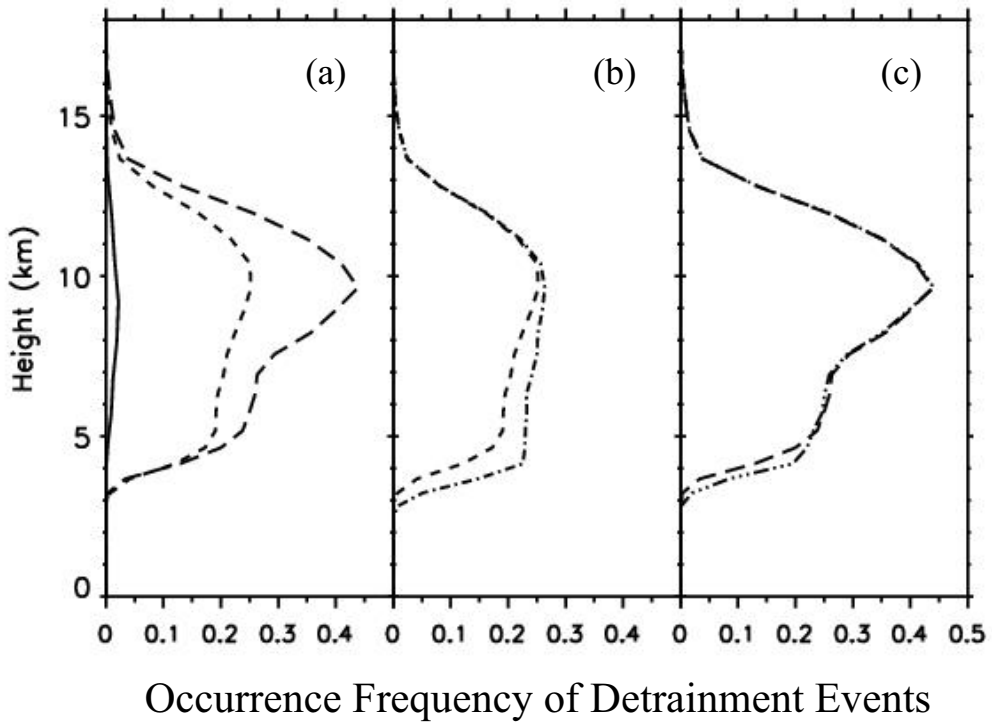

Figure 3. Profiles of occurrence frequency of detrainment events averaged over the entire simulation period in the SCM and CRM simulations. (a) Detrainment of cloud ice in the SCM (solid line), CRM_inact (short-dashed line) and CRM_core (long-dashed line. (b) Detrainment in CRM_inact of cloud ice (short-dashed line), and cloud ice plus snow (dot-dashed line). (c) Detrainment in CRM_core of cloud ice (long-dashed line), and cloud ice plus snow (dot-dashed line).

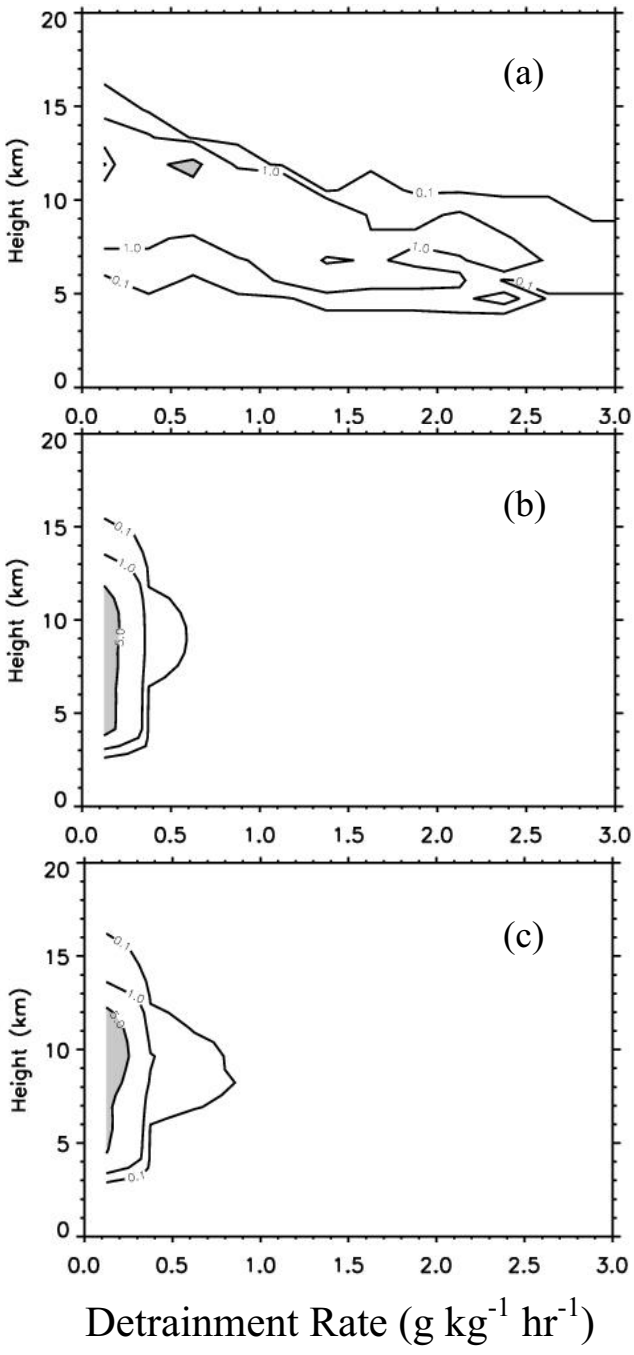

Figure 4. The 2-D histograms of detrainment rate of cloud ice in the SCM (a), and of cloud ice plus snow in CRM_inact (b) and CRM_core (c), respectively. The contours are 0.1, 1.0, 5.0%.

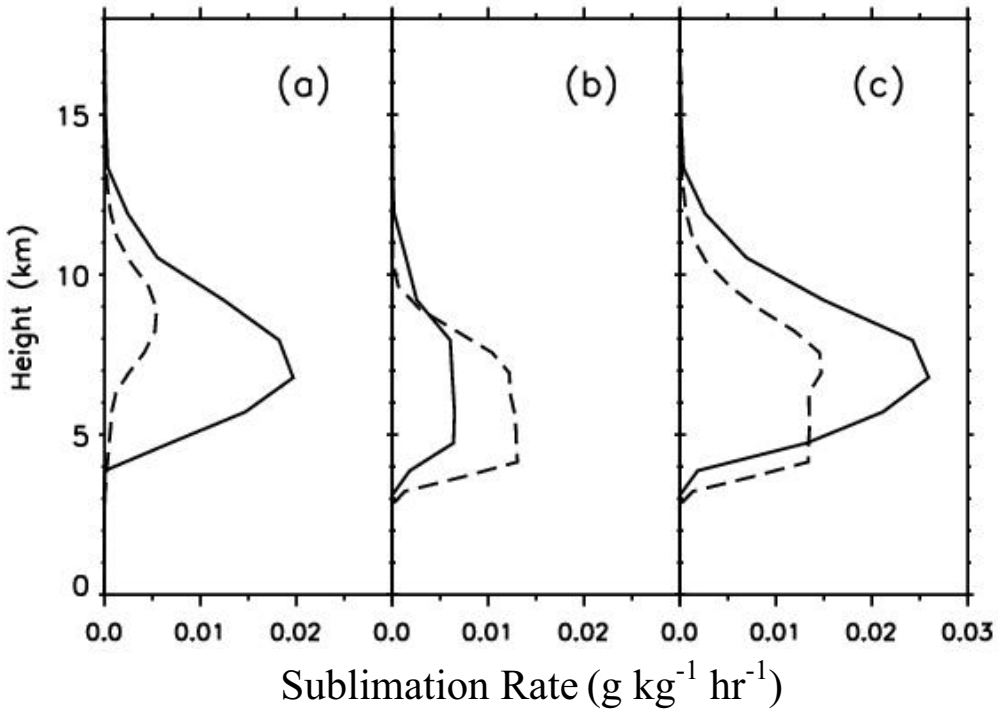

Figure 5. Sublimation rate averaged over the entire simulation period in the SCM (solid line) and CRM (dashed line). (a) Sublimation rate of cloud ice, (b) Sublimation rate of snow, and (c) Sublimation rate of cloud ice plus snow.

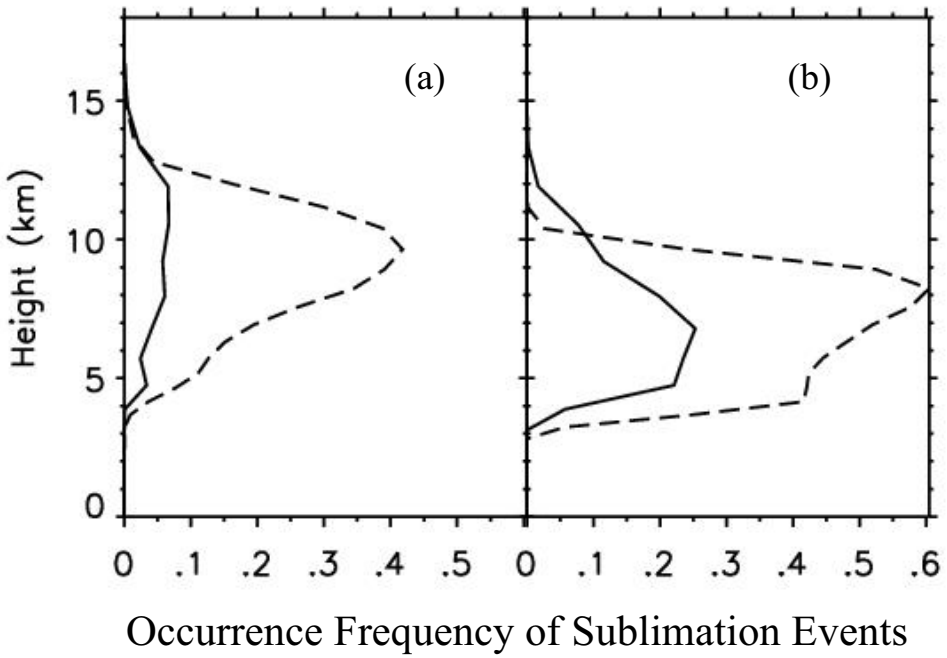

Figure 6. Occurrence frequency of sublimation events averaged over the entire simulation period for (a) the SCM cloud ice (solid line), the CRM cloud ice (dashed line); (b) the SCM snow (solid line), and the CRM snow (dashed line).

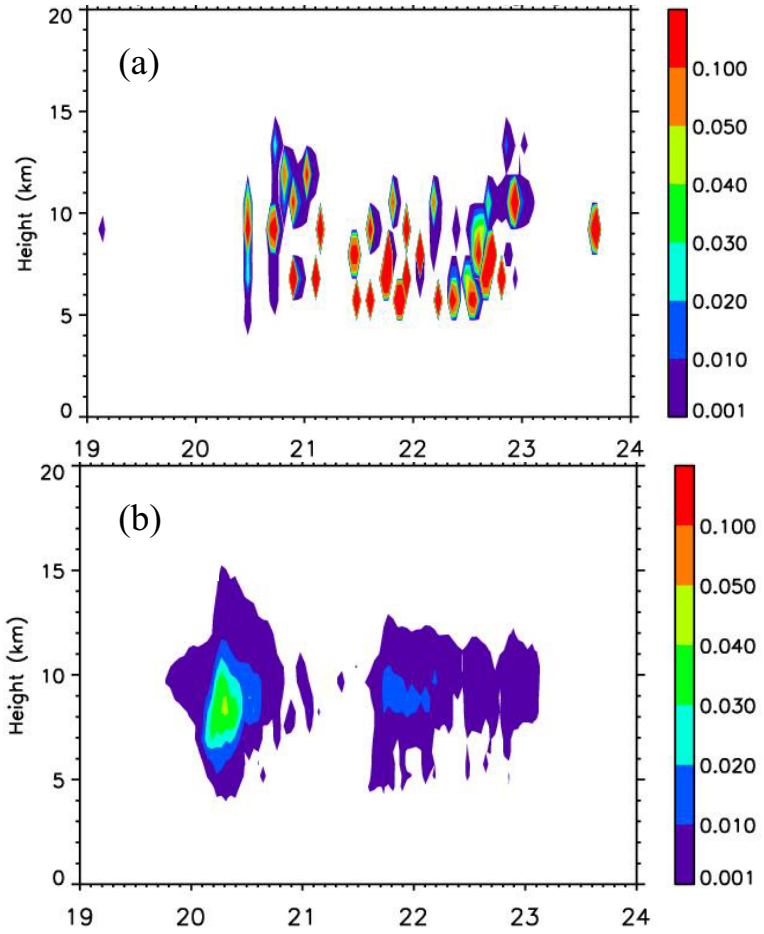

Figure 7. The time-height distribution of hourly averaged sublimation rate of cloud ice in the SCM (a) and CRM (b), respectively. The sublimation rates are in g kg^{-1} hr^{-1}.

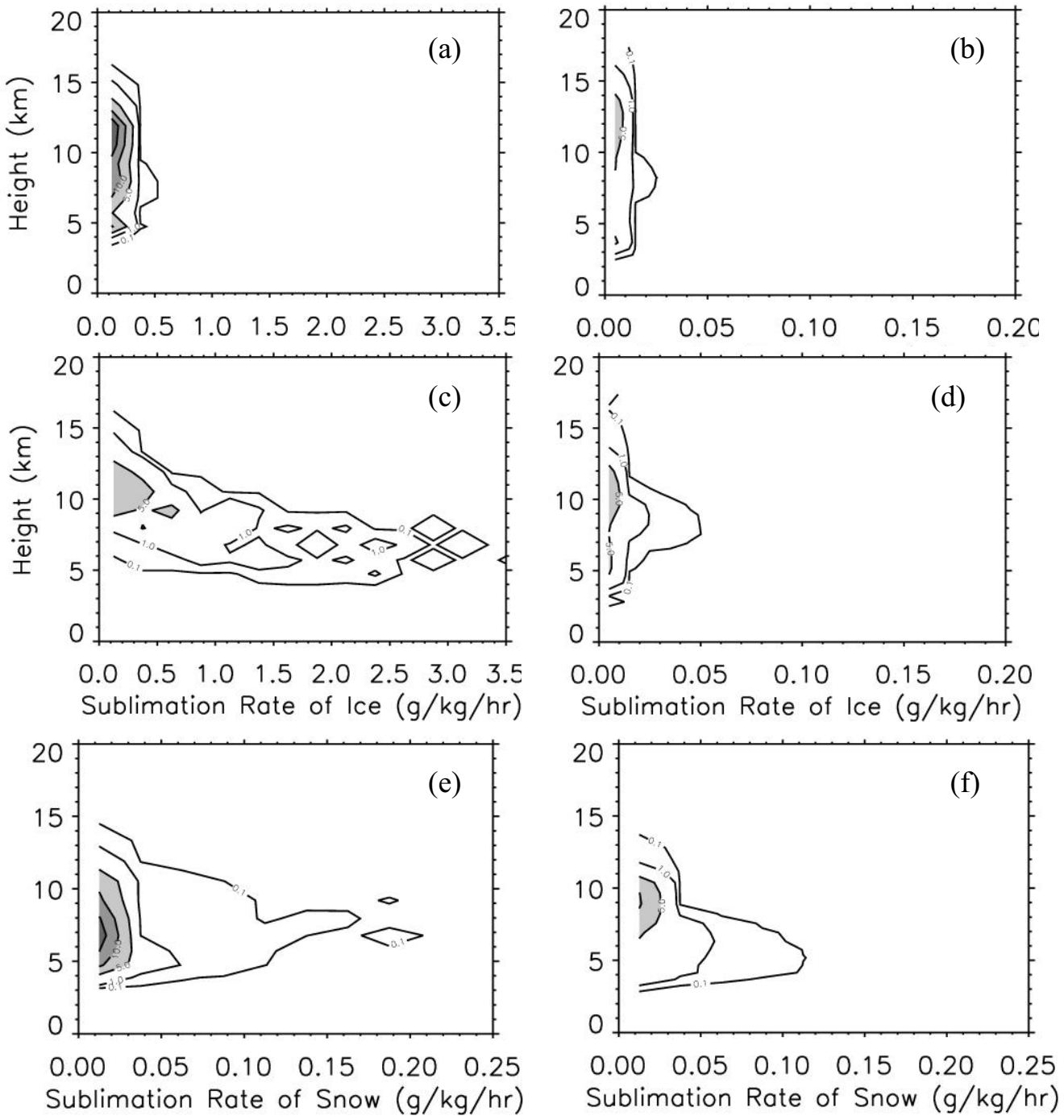

Figure 8. Panels (a) to (d) are 2-D histograms of sublimation rate for cloud ice. Panels (a) and (c) represent sublimation events that occur without and with, respectively, an occurrence of detrainment for cloud ice at the same time and level in the SCM. Panels (b) and (d) are similar to (a) and (c), respectively, but for the CRM. Panels (e) and (f) are 2-D histograms of sublimation rate of snow in the SCM and CRM, respectively. The contours are 0.1, 1.0, 5.0, 10.0, 15.0%.

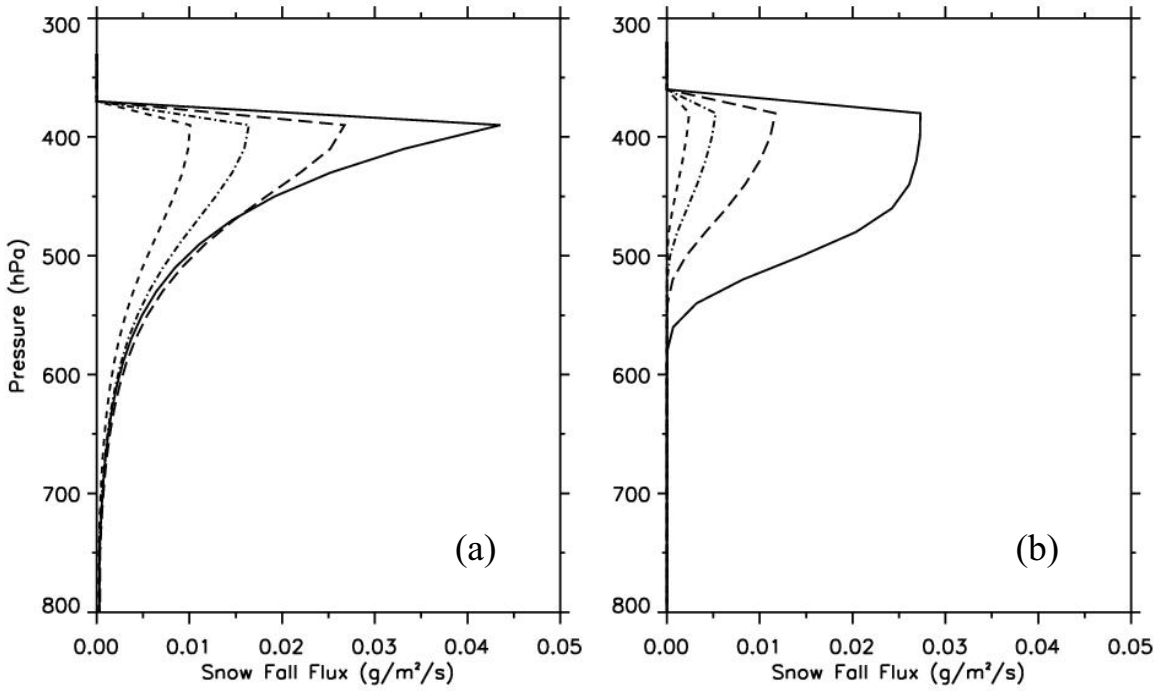

Figure 9. Fall flux of snow simulated by Dscm (a) and Dcrm (b), respectively. The solid, long-dashed, dot-dashed, and short-dashed line represents snow flux at 0.5, 1.0, 1.5, and 2.0 hr, respectively.

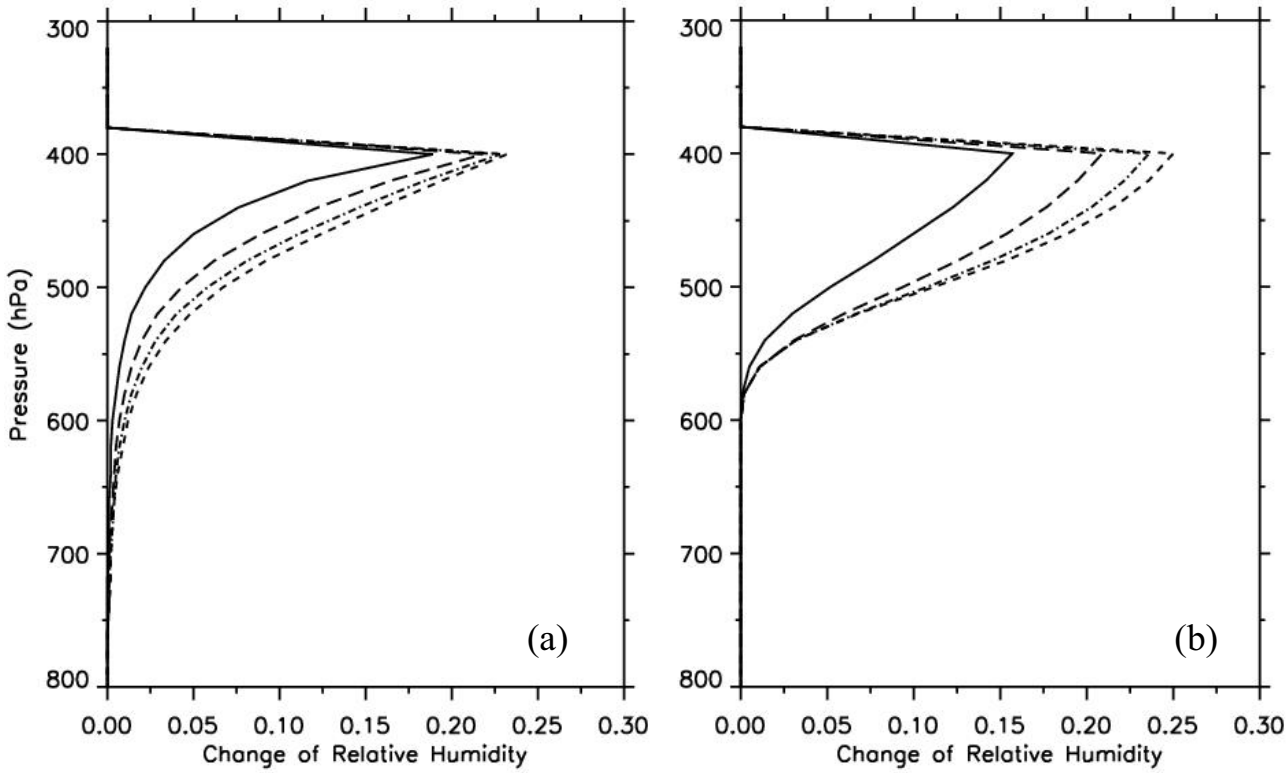

Figure 10. Change of relative humidity from the initial condition simulated by Dscm (a) and Dcrm (b), respectively. The solid, long-dashed, dot-dashed, and short-dashed line represents snow flux at 0.5, 1.0, 1.5, and 2.0 hr, respectively.